A comprehensive study for the airborne gamma-rays spectrometry results of Gabal El-Hassnawia, Central Eastern Desert, Egypt

Ahmed A. NIGM ⓘⓓ, Baher M. GHEITH ⓘⓓ, Mohamed A. SHAHEEN* ⓘⓓ

Nuclear Materials Authority, P.O. Box 530 El Maadi, Cairo, Egypt

Abstract: The present study utilizes the airborne gamma-ray spectrometric data of Gabal El-Hassnawia and its vicinity in an attempt to refine the surface geological mapping and recognize the radioelements occurrences. The statistically analysed surface lineaments derived from the Landsat image proved that they are oriented to the NW, NNW, N–S, and ENE trends. Qualitatively, the highest radiometric levels are related to the younger granites, the intermediate levels are observed over the Hammamat sediments and the acidic metavolcanics while the low levels are coinciding with the metasediments, ultramafites and basic to intermediate metavolcanics. The composite images show a good close correlation with the geologically mapped rock units. The factor analysis proved that the radiometric variables uranium (eU), potassium (K) and thorium (eTh) as well as total count (TC) are highly correlated positively with each other. Three principal factors F1, F2 and F3 are extracted from the data and their scores were used in differentiating the rock types according to their radiometric levels; consequently, nine interpreted litho-radiometric units were identified. Three types of younger granites and two types of Hammamat sediments could be distinguished among the nine units. These units are subjected to statistical treatment with the goal of identifying the uranium occurrences that exceeds $X + 2S$ and $X + 3S$ as targets of exploration. Accordingly, it is found that the uranium province zones are related to the three types of granite (G1, G2 and G3), the second type of Hammamat sediment (H2) and more or less the acidic metavolcanics. The uranium migration indicated that the second type of Hammamat sediment (H-2) is the only unit that the uranium is migrated in whereas; the uranium is migrated out in all other units.

Key words: Gabal El-Hassnawia granitic, uranium migration, factor analysis, composite image

1. Introduction

Aerial gamma-ray spectrometry constitutes an important element for the explanation of the geological units and eventually for the identification of

---

*corresponding author, e-mail: mamshaheen2002@yahoo.com

structures that bound lithologic units. In this way, the method may be specifically important in the discrimination and analysis of granitic bodies. Image processing systems can now be used to enhance and display gamma-ray data so that very slight changes in radioelement concentrations can be mapped. The geologic units in high clear contrast colour can be displayed from the R, G, and B combination of Landsat +7 scene to differentiate the felsic, mafic and wadi deposits. The surface expressions of faults, fractures and lithological boundaries can also be represented from the Landsat data. The geological, geochemical and mineral exploration can be produced from the composite false colour image from gamma-ray spectrometric data. Such images facilitate the spatial correlation of features in the various input data sets (*Broome, 1990*). Reduce the complexity of gamma-ray spectrometric data from seven parameters to three ones is the major goal of the factor analysis technique which helps scientists to define their variables more precisely and decide which of them they should study (*Comery, 1973*). Interpreted Lithological Radiometric Units (ILRU) can be estimated from the statistical treatment of the gamma-ray spectrometric data depending on the calculations of minimum (min.), maximum (max.), arithmetic mean (X) and standard deviation (S) for the all different radiospectrometric parameters of the different rock units.

2. Study area and geological setting

The area of study (Fig. 1) represents the African Orogenic Belt, that was separated from the Arabian shield along the Egyptian Eastern Desert by the Red Sea Graben, and trend mainly NW–SE. It is a part of the Central Eastern Desert of Egypt that was subjected to several activities in the Precambrian rocks due to its long history and varied highly complicated geology. It enclosed between latitudes $25° 39' 00''$ and $25° 49' 20'' \,$N, and longitudes $33° 44' 30''$ and $33° 56' 15'' \,$E.

The exposed rock types of El-Hassnawia area include metamorphic, sedimentary, and igneous rocks (Fig. 2). The metasediments represent the oldest rock unit in the study area. This unit is relatively limited in distribution and appears as moderate to low-relief exposures. *Fowler and Osman (2013)* found that it is exposed in the cores of anticlinal structures and within the uplifted tectonic blocks.
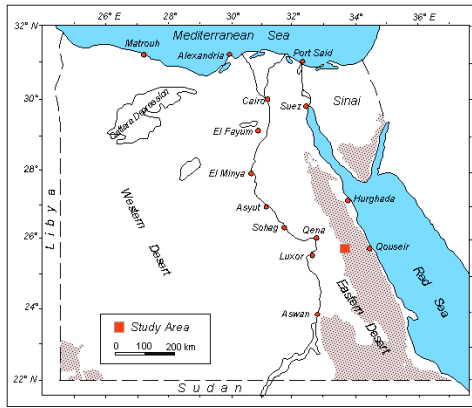
Fig. 1. Map of Egypt showing the location of the study area.
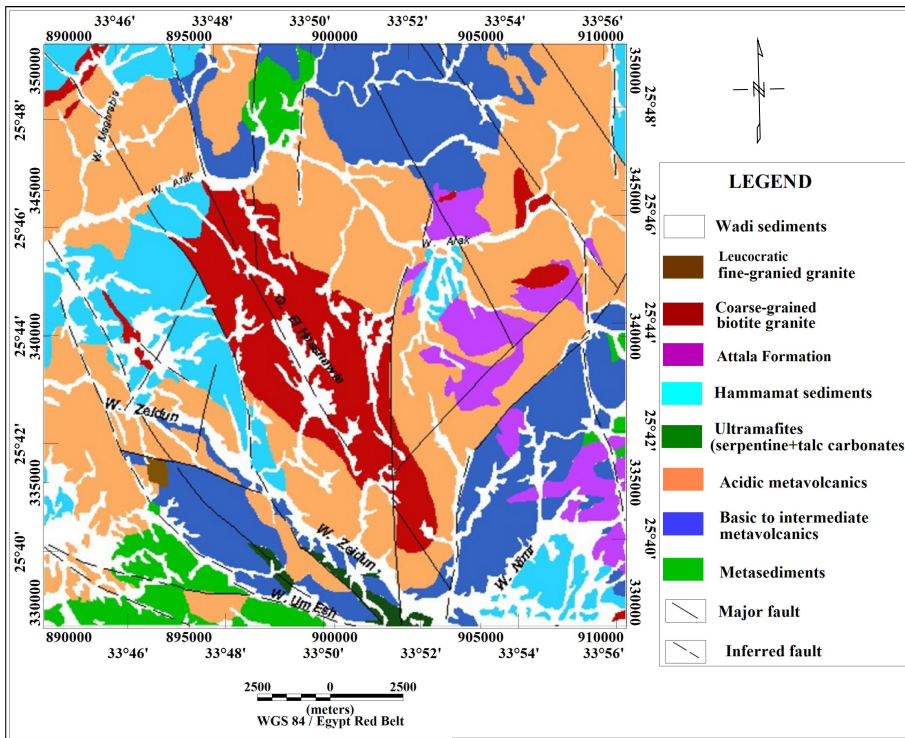
Fig. 2. Compiled geological map of the study area (after *Sabet et al., 1976*).

The metavolcanic flows form thick stratified layers that are interbanded with their pyroclastics. They are categorized into two types: the intermediate, and the acidic metavolcanics (Fig. 2). The basaltic to intermediate metavolcanics are made up of thick flows of metabasalt and meta-andesite with black, pale green to dark grey colours, while the acidic metavolcanics are composed mainly of metarhyolite, metadacite and metarhyodacite with buff, reddish brown to red colours (*Abdel Gawad et al., 2021*). They are banded, jointed, highly foliated, and weathered. The studied metavolcanics are non-conformably upwardly followed by a thick sequences of the Hammamat sediments (*Fowler and Osman, 2013*).

Ultramafites are composed mainly of serpentinites talc-carbonates, and magnesite minerals with a marked enrichment of chromite (*Ali et al., 2021*). They occur as lenses, sheets and belts conformable with the involving metasediments. The serpentinites are fine-grained, soft rocks, cavernous, moderate- to high relief, pale to dark grey, and violet-brown patches. The serpentinites, are exposed to the southern borders, as NW–SE elongated masses associated with the metasediments and metavolcanics of Wadi Um Esh.

Hammamat sediments are widely distributed and cropped out in several localities forming large isolated exposures. *Fowler and Osman (2013)* and *Dessouky et al. (2019)* mentioned that the Hammamat sediments are regionally folded into a major syncline forming a narrow elongated basin trending NW–SE. In the southern part of the basin, minor syncline-anticline folds are observed. Numerous normal faults trending NW–SE with a few following a NE–SW direction run through the sediments.

Post-Hammamat felsites (Attala felsites) form small exposures intruding the Hammamat sediments and the metavolcanics. The Post-Hammamat felsites, together with the subsequent Phase I of the younger granites, were emplaced along NW to NNW trends therefore; the earliest indication of the NNW faults is locally marked by the Post-Hammamat felsites (*Greiling et al., 2014; Fowler and Osman, 2013; Ahmed, 2017; Zoheir et al., 2019*).

Two types of younger granites could be distinguished in the geological map (Fig. 2); coarse-grained biotite granites and leucocratic porphyritic microgranite. The coarse-grained biotite granites form the large granitic mass of El-Hassnawia area. Besides they make up number of small stock shaped masses scattered throughout the investigated territory. *Fowler and Osman (2013)* and *Ahmed (2017)* mentioned that from the structural point

of view, these granites are confined to both blocks and zones of deep faults
and the masses are arranged to the NW–SE direction parallel to the zone
of deep fault Hammamat-Um Naggat. The porphyritic microgranite forms
an irregular small mass south of Wadi Zeidun.

Quaternary sediments including sands, pebbles and rare boulders as a
result of the weathering and denudation processes for the surrounding hills
are filling the wadies. It is observed that the gradual broadness of the wadies
in the area increases westwards and south-eastwards.

3. Methods used and results

The basic data processed during the present study were derived from (i) geo-
logical maps (*Sabet et al., 1976*), (ii) faults lineaments that were interpreted
from the analysis of the geological maps and Landsat images and (iii) the
aerial gamma-ray spectrometric data to determine the surface structures
and lineaments in the study area. The statistical analysis of radioelements
illustrates the high radiation zones and differentiates the boundaries be-
tween rock units. Calculations of uranium mobility were used to determine
the leach in and leach out rocks in the study area.

3.1. Structural background and analysis of surface lineaments

The rock formations of the area of study are present within a NW great
synclinorium structure and fracture lines crossing the area in various trends
affected the distribution of these rock types (*Greiling et al., 2014; Fowler
and Osman, 2013; Ahmed 2017*). The fractures are grouped into two types:
the first "transverse" group traverses the area in the ENE, WNW and E–W
directions, and the second "longitudinal" is a relatively younger including
NNW, NNE, NE trends (*Osman 1996; Greiling et al., 2014; Fowler and Os-
man, 2013; Ahmed 2017*). *Abu El Leil et al. (1977)* recorded that the Late
Proterozoic deep-seated faults separating large consolidated blocks represent
the oldest dislocations forming thick and long zones as magma conducting.
Tectonically, the area can be divided into three major consolidated blocks
separated from each other by deep-seated faults.

Lineaments are the traces of discontinuities such as faults, fractures,
joints and bedding planes with the land surface. These surface features when

properly identified, can usually be assumed to reflect subsurface structures of an area. Thus, the lineaments analysis not only provides a method for detecting past tectonic trends but also helps in the exploration of minerals, oil, and ground water and the seismic hazards for nuclear sites and repository studies as well (*Mostafa and Zakir, 1996*). Figure 3 is a one scene of Landsat +7 covering the selected area (30 cm resolution). Displayed in R, G, and B represents the geologic units in high clear contrast colour. False colour composite image of band combination 7, 4, 2 in R, G and B is used for representing the rock unit boundaries in the selected area. This combination shows the variation of felsic, mafic and Wadi deposits. They may represent the surface expressions of faults, fractures and linear lithological boundaries or escarpments. A great number of fracture lines in the basement rocks are shown in the Landsat image.
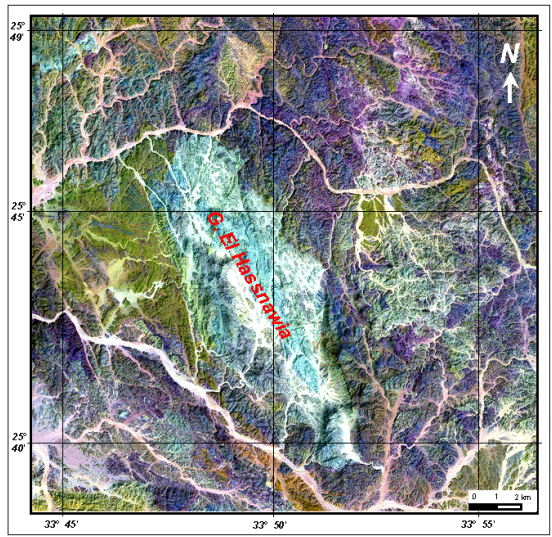

Fig. 3. Landsat image of the study area.

Statistical analysis of the structural lineaments (Fig. 4a) of the Landsat images of this area resulted in acquisition of statistical data on the number, length, and the orientation of the lineaments. These statistics allowed constructing the rose diagrams (Fig. 4b) which explains the surface structural setting of the area. The statistical analysis results show that most of the structural lineaments are oriented to the NW, N–S, NNW and ENE trends.
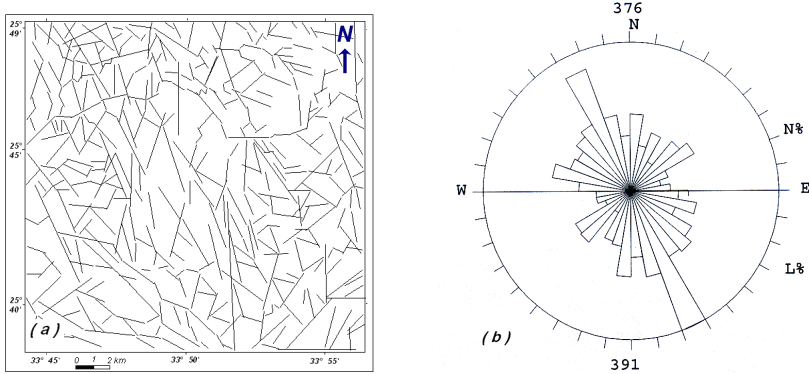
Fig. 4. Surface lineaments (a) and Rose diagram of the study area (b).

3.2. Airborne gamma-ray survey

The province of the Eastern Desert of Egypt including the area of study provides a good example of the application of airborne γ-ray spectrometry. This is because most of the Eastern Desert of Egypt lacks soil or vegetation cover and the screening effects of the radiation field is negligible and airborne radiometry provided very dependable information for significant mineralization. Moreover, the region characterizes by minimal chemical weathering (*Rabie et al., 1996*).

The area of study has been included in the systematic airborne survey conducted by Aero-Service Division, Western Geophysical Company of America in 1984. The survey was carried out along NE–SW parallel flight lines at one kilometer line spacing and 120 m ground clearance. A high sensitivity 256 channel airborne gamma-ray spectrometer was used to carry out the survey (*Aero-Service, 1984*). Such surveys define geophysical anomalies that are of interest for exploration. The corrected total count measurements were converted into units of radioelement concentration (Ur) as recommended by the International Atomic Energy Agency (*IAEA, 1976*).

3.2.1. Qualitative interpretation

The qualitative interpretation of the aerospectrometric maps of the study area depends mainly upon the correlation between the general pattern of the recorded aeroradioactivity measurements and the surface distribution

of the various types of rock units in general, and the basement rock units in particular.

3.2.1.1. Radioelement contour maps

Contour maps were generated for total count (TC), equivalent uranium (eU), equivalent thorium (eTh) and potassium (K). These maps as well as the ratio maps of K, eU and eTh are used for subsequent interpretation of the airborne gamma-ray data to aid in the visual interpretation of potential exploration areas. Detailed visual analysis of these spectrometric maps (Figs. 5 to 11) emphasizes the spatial nature of the radioelement distribution correlating with the geological and structural features which have important spatial characteristics. Consequently, the relationship of the contoured radioelement patterns and the distribution of the major anomalous lithologies have formed the basis for the present interpretation.

Careful examination of a spectrometric map shows the considerable differentiation in the radiometric levels of the mapped geologic units. The higher radiometric levels in this area are significantly comparable with the younger granite of El-Hassnawia pluton. The oval shape of the highly anomalous zone make it is easy to recognize, identify and outline the lithological boundaries of the pluton due to the overall changes in the radiation and the high contrast in the radiometric signature of this unit with the other adjacent lithologies as shown on the maps. Major radiometric variations are nevertheless noted within the massif pluton. On the whole, the highest levels are in the center and outwards decreasing towards the rim.

Generally, there is a good agreement between mapped geological boundaries of El- Hassnawia granitic pluton and those defined by the high aeroradioactivity surveyed data. The intermediate radiometric response was observed as associated with the Hammamat sediments and the acidic metavolcanics while the low levels are coinciding with the metasediments, ultramafites and basic to intermediate metavolcanics.

The total count (Fig. 5) ranges from 0.9 over the metasediments to 26.2 Ur over El-Hassnawia younger granite. The eU content (Fig. 6) reaches to 7.3 ppm as maximum value over El-Hassnawia younger granite and diminishes to 0.13 ppm (minimum value) over the metasediments. The eTh content (Fig. 7) recorded 23.7 ppm as maximum value over El-Hassnawia
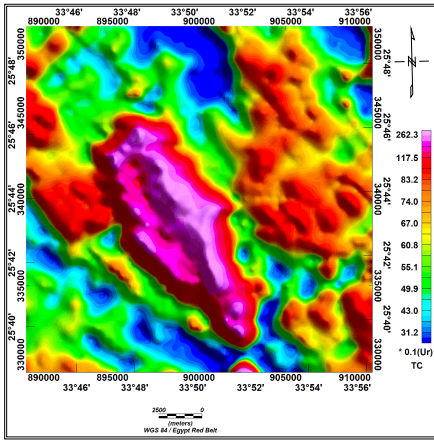
Fig. 5. Total Count filled colour contour map in Ur.
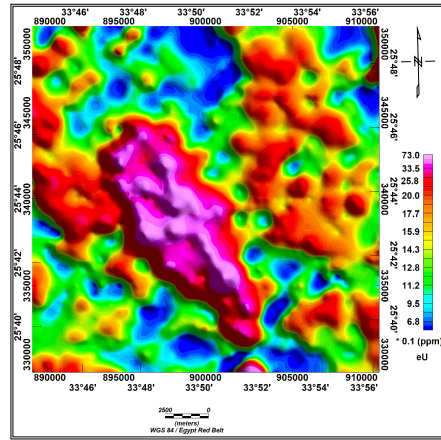
Fig. 6. Equivalent Uranium (eU) filled colour contour map in ppm.
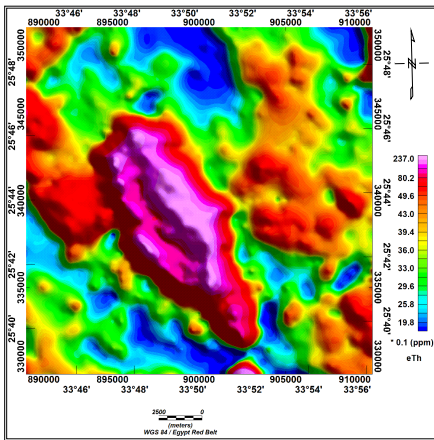
Fig. 7. Equivalent Thorium (eTh) filled colour contour map in ppm.
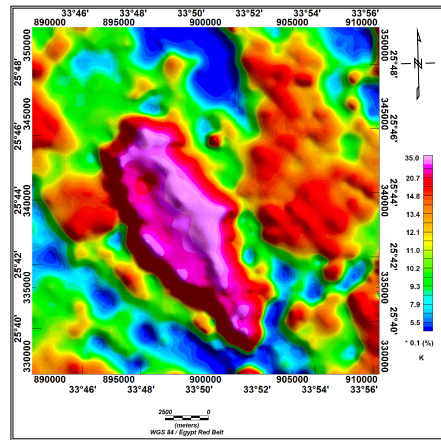

Fig. 8. Potassium (K) filled colour contour map in %.

younger granite and 0.9 ppm (minimum value) over the metasediments. The potassium (Fig. 8) content ranges from 0.2% over the metasediments to 3.5% over El-Hassnawia younger granite.

Ratio maps can enhance subtle variations in the measured variables. The eU/eTh and eU/K maps (Figs. 9 and 10) show the lowest values
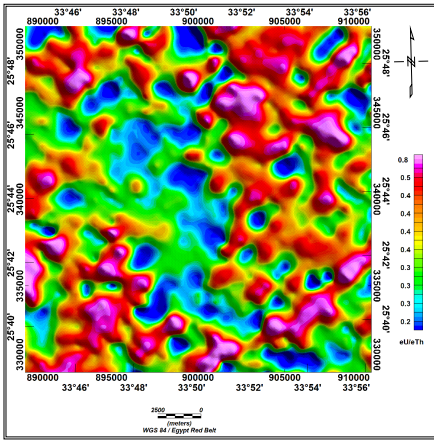
Fig. 9. eU/eTh filled colour contour map.
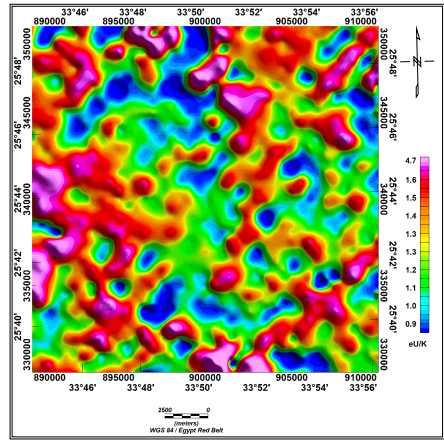
Fig. 10. eU/K filled colour contour map.
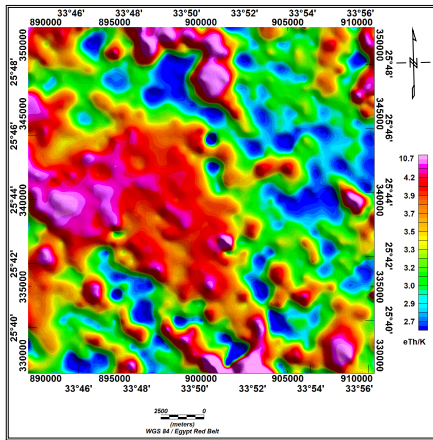
Fig. 11. eTh/K filled colour contour map.

over the Hammamat sediments, basic to intermediate metavolcanics and El-Hassnawia younger granites whereas the highest values are correlated to the acidic metavolcanics. The lowest radiometric values of the eTh/K map (Fig. 11) are observed over the acidic metavolcanics and metasediments while, the highest levels are coinciding with granitic plutons and Hammamat sediments.

404

3.2.1.2. Composite imaging

Combination information from two or more data sets into a single display creates composite colour images. Such images facilitate the spatial correlation of features in the various input data sets (*Broome, 1990*). The most common type of image is a colour-coded intensity image produced by assigning different colours to grid cells based on the magnitude of the geophysical parameter. Displaying geophysical data in image form can often reveal information that is hidden in contour or profile maps (*Cordell and Knepper, 1987*). Composite false colour image particularly produced from gamma-ray spectrometric data provides an interpreter with a useful synthesis of the data that can be used to aid geological and geochemical mapping and mineral exploration.

The ternary (three-component) radioactive element map is an effective method of displaying variations in total radioactivity and in the relative abundances of the three radioactive elements. The radioelement composite image provides a view of the overall pattern of the three elements and usually contains patterns related to various lithologies. However, four composite colour image maps were prepared as K, eU and eTh (three radioelement composite image map), eU, eU/eTh and eU/K (equivalent uranium composite image map), eTh, eTh/eU and eTh/K% (equivalent thorium composite image map) and K, K/eU and K/eTh (potassium composite image map).

a. Absolute radioelement composite image

Different rock types have different characteristic concentrations of the three main radioelements, K, eU and eTh. Therefore, concentrations calculated from γ-ray spectrometric data can be used to identify zones of consistent lithology and contacts between constraining lithologies. Three-element display of eU (in ppm), eTh (in ppm), and K (in %) of the study area (Fig. 12) shows variations which mainly reflect the different lithologies. The colour index at each corner of the triangular legend (K in red, eTh in green and eU in blue) indicates 100% concentration of the indicated radioelement. Colours at each point inside the triangle represent different ratios of the radioelements according to their colour differences on the absolute three radioelement composite image map. The eU, eTh and K images emphasize the radioelement and highlight areas where the particular radioelement has relatively higher concentrations. Areas of the image with the same colour

will have similar ratios of K, eU, eTh, and the intensity of that colour is a measure of the total radioactivity. This allows the map to represent the radioactive element distribution better than any of the other single variable maps.

It was noticed that the observed radioelement zones show a good close spatial correlation with the geologically mapped lithologies (Fig. 2). The bright higher radioelement concentration zones are clearly correlated with El-Hassnawia younger granite, two small poses to the east, Hammamat sediments and more or less with acidic metavolcanics. Low eU, eTh and K concentrations (black areas) show small scattered spots correlated with the metasediments, ultramafites and basic to intermediate metavolcanics. The younger granites of El-Hassnawia pluton, which are normally characterized by their relatively high radiometric response, are clearly visible on the absolute radioelement composite image map. This pluton can be easily discriminated from the adjacent rocks, which are relatively low in radioactivity.

b. Equivalent uranium composite image

The eU composite image map (Fig. 13) combines eU (in red) with ratios eU/eTh (in green) and eU/K (in blue). The relative concentration of eU with respect to both K and eTh is an important diagnostic factor in the recognition of possible uranium deposits (*IAEA, 1988*). Therefore, this map could assist in identifying the anomalous zones of enriched uranium concentration. Examination of this image (Fig. 13) shows clear red colour characterizes the oval shape of the younger granite pluton, that is because the high concentrations of the three radioelements relative to each other on that pluton. It was noticed that the bright colour which refers to high eU concentrations relative to both of eTh and K represents linear features correlated mainly with the wadies either in the pluton or in the surroundings. Also, bright anomalous zones on certain lithologies are limited in their spatial distribution forming local scattered spots, which may reflect inhomogeneities in the composition of the corresponding lithological units.

c. Equivalent thorium composite image

The eTh composite image map (Fig. 14), combines eTh (in red), eTh/eU (in green) and eTh/K (in blue). This image emphasizes the relative distribution of eTh and highlight areas of thorium enrichment. Bright colour on

this image is a good pointer to areas where thorium has been preferentially enriched relative to potassium and uranium. These bright-coloured zones are correlated well with El-Hassnawia pluton as well as some small scattered spots associated mainly with Hammamat sediments.

d. Potassium composite image

The potassium (K) composite image map (Fig. 15) combines K (in red) with K/eTh (in green) and K/eU (in blue). This image shows the overall spatial distribution of the relative potassium concentrations. High relative potassium concentrations can be distinguished on the potassium composite image map as anomalous zones (high values) correlated essentially with El-Hassnawia granitic pluton and the Hammamat sediments.

3.2.2. Analysis techniques and quantitative interpretation

The quantitative treatment of the spectrometric data in the present study is discussed on the light of factor analysis and uranium migration techniques with the statistical treatment as well. It depends principally upon the fact that, the absolute and relative concentrations of the radioelements (eU, K and eTh) vary measurably and significantly with lithology (*Darnley and Ford, 1989*).

3.2.2.1. Factor analysis

The factor analysis is a multivariate statistical technique which helps scientists to define their variables more precisely and deciding which of them they should study (*Comery, 1973*). One of the major goals of factor analysis is to reduce the complexity of data matrices (*Klovan, 1968*) where, the number of variables is reduced to the minimum number of independent variables which adequately describes the data. *Duval (1976)*, *Wecksung (1982)*, *Mostafa (1988)* and *Mostafa et al. (1990)* applied this technique to the airborne gamma-ray spectrometric data since it allows the geologist/geophysicist to perform a coordinate transformation from the four count rates (K, eU, eTh, and TC) with the three ratios (eU/eTh, eU/K, and eTh/K) to a system of three independent coordinates. These three coordinates are constrained to reproduce the total variance of the original data, and the data can be separated into groups using the criterion that similar data points have similar
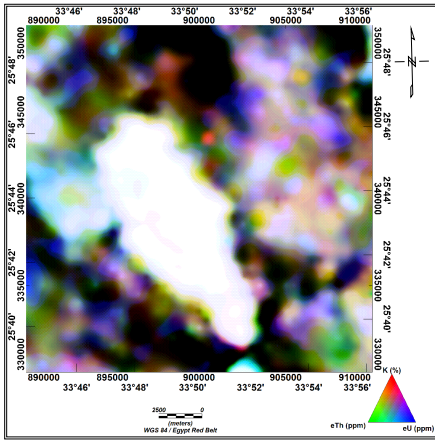
Fig. 12. False colour radioelement composite image.
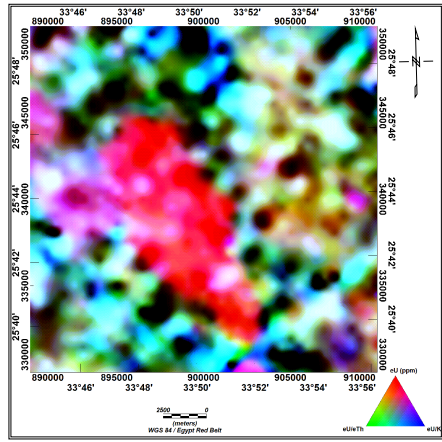
Fig. 13. False colour eU composite image.
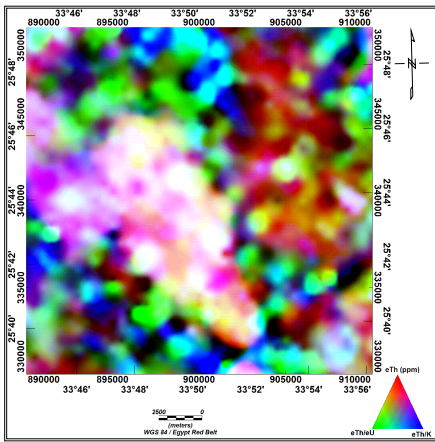
Fig. 14. False colour eTh composite image.
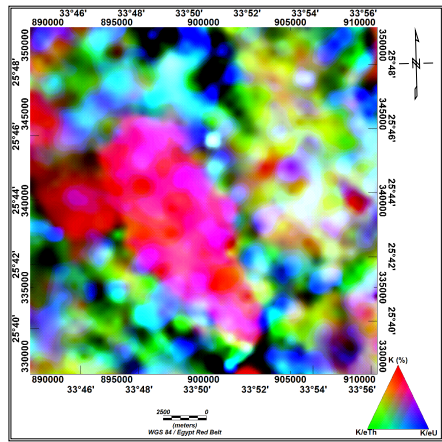
Fig. 15. False colour K composite image.

coordinates. The distribution of the separated groups can be mapped for comparison with other information such as the mapped geology. This map represents a synthesis of all of the radiometric data.

The factor analysis computation involves three major steps: (i) the correlation matrix, (ii) factor extraction and (iii) factor rotation. The corre-

lation matrix indicates to some extent that these variables are related to each other or overlap in what they measure. The factor extraction determines how many factors constructs are needed to account for the pattern of values found in the correlation matrix. This process involves a numerical procedure that uses the coefficients in the (R) matrix to produce factor loadings. Some variables might have a substantial negative loading on the factor, indicating that it is negatively correlated with the factor construct. The so-called rotational process in factor analysis involves finding a factor matrix into another form that will represent an optimum set of constructs.

The correlation matrix of the spectrometric variables of the study area is calculated and presented in Table 1. Three principal factors F1, F2 and F3 are extracted from the data after being rotated using the Varimax method (Table 2). The computed score values of the three factors are represented as two-dimensional score contour maps for F1, F2 and F3 (Figs. 16, 17

Table 1. Correlation coefficient between the seven data variables.

Variables	TC (Ur)	eU (ppm)	eTh (ppm)	K%	eU/eTh	eU/K	eTh/K
TC (Ur)	1.00						
eU (ppm)	0.94	1.00					
eTh (ppm)	0.98	0.91	1.00				
K%	0.98	0.90	0.95	1.00			
eU/eTh	−0.22	0.05	−0.32	−0.26	1.00		
eU/K	−0.07	0.21	−0.06	−0.18	0.74	1.00	
eTh/K	0.24	0.28	0.39	0.12	−0.29	0.41	1.00

Table 2: Varimax factor loadings matrix for the seven variables.

Variables	Component		
	F1	F2	F3
TC (Ur)	0.988	0.011	0.134
eU (ppm)	0.929	0.305	0.155
eTh (ppm)	0.995	−0.005	−0.041
K %	0.966	−0.089	0.220
eU/eTh	−0.299	0.822	0.479
eU/K	−0.061	0.979	−0.172
eTh/K	0.355	0.287	0.888

and 18) respectively. Investigation of Table 1 shows that the total count (TC) is highly correlated positively with eU (94%), eTh (98%) and K (98%) and weakly correlated with eU/eTh, eU/K and eTh/K as −0.22, −0.07 and 0.24 respectively. The eU is highly correlated with eTh (91%) and K (90%), weakly correlated with eU/K (21%) and eTh/K (28%) and very weakly correlated with eU/eTh (5%). The eTh is highly correlated with K (95%). It is weakly correlated with eTh/K (39%) and inversely correlated with eU/eTh (−32%) and eU/K (6%). The K is weakly correlated with ratios eU/eTh (26%), eU/K (18%) and eTh/K (12%). The ratio eU/eTh is highly correlated with eU/K (74 %) and negatively correlated with eTh/K (−29%). The eU/K is moderately correlated with eTh/K (41%).

Table 2 shows the three principle factors F1, F2 and F3 that extracted from Table 1 after their rotation using the Varimax method. It can be noticed from these tables that F1 has an appreciably high positive loading with the four variables TC (98%), eU (92%), eTh (99%) and K (96%). The second factor F2 is positively highly loaded with ratios eU/eTh (82%) and eU/K (98%) while it is weakly positive loaded with eU (31%) and eTh/K (29%). F2 is inversely loaded with eTh and K. The third factor F3 is moderately positive loaded with eU/eTh (48%) and weakly positive loaded with TC (13%), eU (15%) and K (22%). On the other hand it is inversely loaded with eTh, eU/K and eTh/K.

The computed scores values of the three factors are represented here as two-dimensional score contour maps for F1, F2 and F3 respectively (Figs. 16, 17 and 18). The first factor F1 can be recalled as a factor of integrated radioactivity or the factor of uranium exploration (*Mostafa et al, 1990*). F1 (Fig. 16) exhibits radioelement concentration zones clearly correlated with El-Hassnawia younger granite, Hammamat sediments and acidic metavolcanics. The second factor F2 and the third factor F3 are recalled as factors of differentiating rock types. The quite inspection and interpretation of the three maps help in delineating and outlining the different units that possess significant or even insignificant levels of radioactivity according to their characterizing factor scores. These units are named in the light of the published geologic map (Fig. 2). The distribution of the rock units, from the radiometric point of view, can be easily distinguished as differences in the score values, where the high score values reflect areas of high radioelement contents and vice versa.
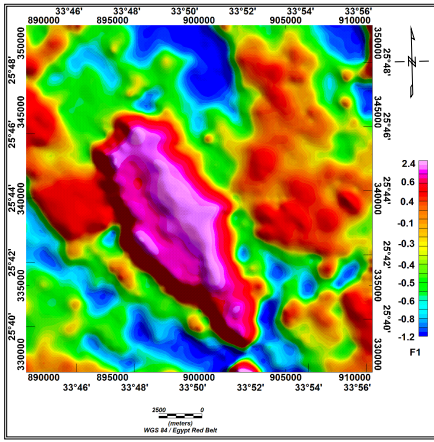
Fig. 16. First factor (F1).
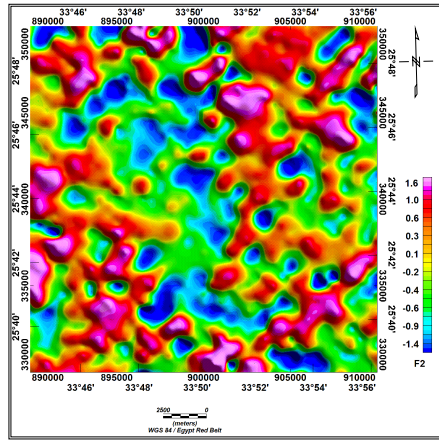
Fig. 17. Second factor (F2).
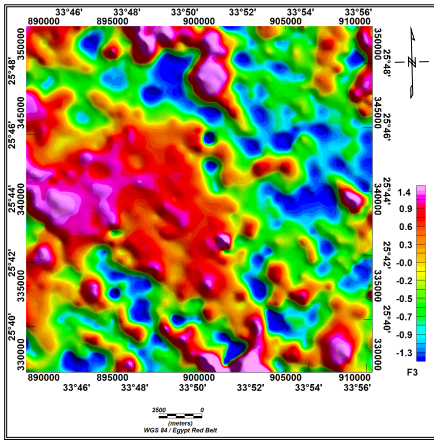
Fig. 18. Third factor (F3).
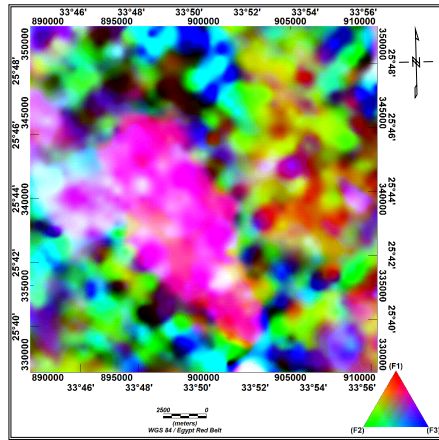
Fig. 19. Ternary plot of F1, F2 and F3.

Clustering these three factors (F1, F2 and F3) together in a ternary composite image map (Fig. 19) is expected to give better information for interpretation. It could be utilized in the geochemical mapping of major rock units. When it is well examined together with the three factor scores maps (Figs. 16, 17 and 18) as well as the geological map (Fig. 2), it separates some rock units effectively as those inferred from the geological map, while others were hard to be differentiating in a comparison with

the surface litho-stratigraphic map of the study area. So, the interpreted surface litho-radiometric unit map is generated as shown in (Fig. 20) from the gamma-spectrometric point of view. It could be easily to recognize nine litho-radiometric units in the map with reasonable degree of correlation with those found in the geologic map.

The interpreted litho-radiometric unit (ILRU) map (Fig. 20) extracted from the false colour composite image map of F1, F2 and F3 (Fig. 19), reflects a distinct content of radioelements for each of the interpreted litho-radiometric units, and probably, common features that could be found in the lithological composition for each unit. Consequently, the identity and contacts of some mapped rock exposures or units were ascertained through the generation of ILRU map, while others were modified, subdivided, or merge two or more rock units in one or partially corrected on the basis of their radioelement (geochemical) content.
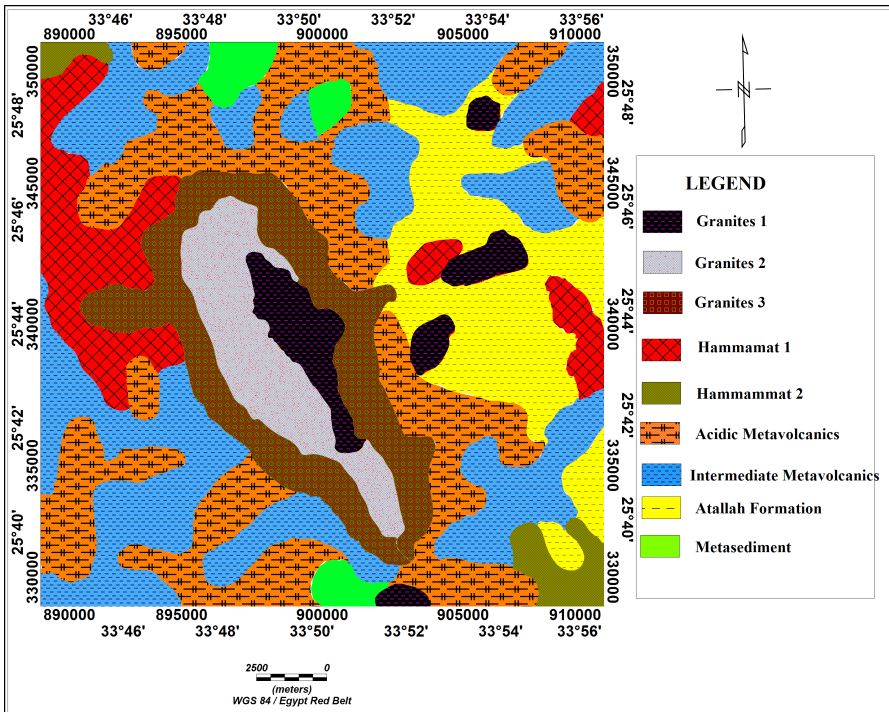

Fig. 20. Interpreted litho-radiometric units map (ILRU).

3.2.2.2. Statistical treatment

The gamma-ray spectrometric survey data have been subjected to statistical analysis in terms of the individual interpreted radiometric lithological units (ILRU) in order to draw valid conclusions and extract reasonable predictions regarding the nature and significance of the distribution of the radioelements in the area. It is worthy to mention that statistical analysis of the aerial spectrometric data has been performed in terms of the individual rock types to avoid errors in geological mapping. Statistical computations were applied on the original data without employing any type of transformation. In this regard, minimum (min.), maximum (max.), arithmetic mean (X) and standard deviation (S) were computed for the different radio-spectrometric parameters for the different rock units. In addition to, the normality and the degree of homogeneity of the radioelements distributions has been tested by the calculation of the coefficient of variability (C.V. $= S/X * 100$) for each radiometric parameter of the different rock types. If C.V.% value of a certain unit is less than 100%, the unit exhibits normal distribution (*Sarma and Kock, 1980*).

Table 3 summarizes the statistical treatment, which applied on the various interpreted lithological radiometric units (ILRU) for the different radiospectrometric variables. Fig. 20 illustrates the ILRU of these variables and their correspondence rock units.

3.2.3. Uranium provinces

The major objective of aerial reconnaissance gamma-ray spectrometric survey data interpretation is to define the probable boundaries of potential uraniferous provinces, in which the rocks and soils are preferentially enriched in uranium (*Saunders and Potts, 1976*). Once these target areas are determined, further detailed ground prospecting methods can be carried out to evaluate their economic importance. From the exploration point of view, the most important parameters, which can be measured, are the relative concentration of uranium to thorium and uranium to potassium taken in conjunction with the uranium measurements. They are diagnostic for identification of zones of anomalous uranium concentration (*Darnley, 1973*).

These zones could be delineated on the basis of calculation of probabilities that the data differ from the mean background as defined by the

Table 3. Statistical analyses of the radioelements in the interpreted litho-radiometric units.

I.L.R.U.	No.	Variables	Min. * 0.1	Max. * 0.1	X * 0.1	S * 0.1	CV%	$X + 2S$ * 0.1	$X + 3S$ * 0.1
G1	73	TC (Ur)	28.22	212.00	136.88	56.37	41.18	249.62	305.98
		eU (ppm)	8.00	56.00	28.24	13.09	46.36	54.42	67.51
		eTh (ppm)	24.00	142.00	94.28	42.83	45.43	179.94	222.77
		K (%)	5.50	35.00	24.32	9.51	39.08	43.34	52.84
		eU/eTh	0.16	0.44	0.31	0.06	19.66	0.43	0.49
		eU/K	0.63	2.80	1.16	0.35	30.39	1.87	2.22
		eTh/K	2.52	7.50	3.80	0.77	20.36	5.35	6.12
G2	103	TC (Ur)	132.80	187.58	162.57	10.08	6.20	182.74	192.82
		eU (ppm)	26.00	51.00	35.65	4.73	13.26	45.10	49.82
		eTh (ppm)	76.00	136.00	113.39	10.53	9.29	134.46	144.99
		K (%)	18.50	33.40	28.91	2.02	6.98	32.95	34.97
		eU/eTh	0.23	0.48	0.32	0.04	13.88	0.40	0.45
		eU/K	0.88	1.85	1.24	0.18	14.57	1.60	1.78
		eTh/K	3.31	4.63	3.92	0.26	6.58	4.44	4.70
G3	172	TC (Ur)	23.24	180.94	100.10	37.47	37.43	175.05	212.52
		eU (ppm)	4.00	48.00	21.60	8.33	38.55	38.25	46.58
		eTh (ppm)	20.00	134.00	67.79	27.68	40.83	123.15	150.83
		K (%)	4.50	32.00	17.85	6.52	36.49	30.88	37.40
		eU/eTh	0.19	0.51	0.33	0.07	19.98	0.46	0.53
		eU/K	0.80	1.74	1.22	0.22	18.09	1.66	1.88
		eTh/K	2.06	6.67	3.76	0.54	14.23	4.83	5.37
H1	142	TC (Ur)	39.84	116.80	76.12	14.68	19.28	105.47	120.14
		eU (ppm)	7.00	29.00	19.17	4.60	23.98	28.36	32.96
		eTh (ppm)	23.00	84.00	50.50	12.42	24.60	75.35	87.77
		K (%)	8.00	18.80	12.82	2.22	17.34	17.27	19.49
		eU/eTh	0.27	0.63	0.38	0.06	15.60	0.50	0.56
		eU/K	0.82	2.36	1.50	0.29	19.38	2.08	2.37
		eTh/K	2.60	5.40	3.92	0.56	14.38	5.05	5.61
H2	37	TC (Ur)	48.96	84.66	65.56	10.53	16.07	86.63	97.16
		eU (ppm)	6.50	22.50	13.51	3.71	27.45	20.92	24.63
		eTh (ppm)	35.00	48.00	43.19	3.41	7.89	50.00	53.41
		K (%)	8.00	14.50	11.30	1.91	16.87	15.12	17.02
		eU/eTh	0.16	0.47	0.31	0.07	23.49	0.46	0.53
		eU/K	0.65	1.63	1.19	0.24	20.00	1.67	1.91
		eTh/K	3.07	5.13	3.90	0.54	13.87	4.98	5.52

Table 3. Continuation from the previous page.

I.L.R.U.	No.	Variables	Min. * 0.1	Max. * 0.1	X * 0.1	S * 0.1	CV%	$X + 2S$ * 0.1	$X + 3S$ * 0.1
A.M.V.	429	TC (Ur)	11.62	99.20	47.62	13.38	28.09	74.37	87.74
		eU (ppm)	1.30	23.00	10.03	3.48	34.67	16.99	20.46
		eTh (ppm)	11.00	65.00	29.67	7.77	26.18	45.20	52.97
		K (%)	3.00	19.50	8.99	2.56	28.47	14.10	16.66
		eU/eTh	0.08	0.60	0.34	0.09	25.25	0.51	0.60
		eU/K	0.28	2.29	1.13	0.30	26.88	1.74	2.05
		eTh/K	1.67	5.45	3.38	0.53	15.80	4.45	4.98
I.M.V.	420	TC (Ur)	14.94	94.62	54.52	13.28	24.36	81.08	94.36
		eU (ppm)	3.00	24.00	14.31	3.78	26.41	21.86	25.64
		eTh (ppm)	8.50	52.00	31.39	7.07	22.52	45.53	52.60
		K (%)	3.50	20.00	9.82	2.50	25.47	14.82	17.32
		eU/eTh	0.13	0.76	0.46	0.10	20.68	0.65	0.75
		eU/K	0.47	2.95	1.49	0.33	22.39	2.15	2.48
		eTh/K	1.89	4.90	3.25	0.45	13.75	4.15	4.59
At. Fm.	198	TC (Ur)	51.46	106.24	77.09	10.13	13.14	97.35	107.48
		eU (ppm)	9.50	25.00	17.46	3.00	17.16	23.45	26.45
		eTh (ppm)	30.00	63.50	42.65	5.56	13.04	53.78	59.34
		K (%)	9.50	19.00	14.18	1.87	13.16	17.92	19.78
		eU/eTh	0.24	0.68	0.41	0.07	16.02	0.54	0.61
		eU/K	0.69	1.91	1.24	0.19	15.27	1.62	1.80
		eTh/K	2.43	4.05	3.02	0.29	9.68	3.61	3.90
M.S.	41	TC (Ur)	9.96	48.64	28.74	9.18	31.92	47.09	105.73
		eU (ppm)	2	18	8.34	2.89	34.61	14.12	105.82
		eTh (ppm)	9	27.5	19.24	4.51	23.45	28.27	79.36
		K (%)	1.5	9	4.75	1.77	37.16	8.28	112.99
		eU/eTh	0.22	0.68	0.43	0.11	25.49	0.65	76.70
		eU/K	0.5	4.8	1.91	0.78	40.80	3.46	122.90
		eTh/K	2.25	7.33	4.34	1.04	23.97	6.42	74.16

Explanation: No. = number of readings, I.L.R.U. = interpreted litho-radiometric unit, X = arithmetic mean, S = standard deviation, CV% = coefficient of variability, Min. = minimum value, Max. = maximum value, A.M.V. = acidic metavolcanics, At. Fm. = Attala Formation, G1 = Granite 1, G2 = Granite 2, G3 = Granite 3, H1 = Hammamat Formation-1, H2 = Hammamat Formation-2, I.M.V. = intermediate metavolcanics, M.S. = metasediments.

data themselves. These differences were computed in terms of certain levels of probabilities. The threshold value which is the beginning of the high anomalous values was considered as the value equaling two or three standard deviations above the calculated arithmetic mean value ($X + 2S$ or $3S$) in each rock unit for eU, eU/eTh and eU/K measurements as given in Table 3. This acceptable threshold was chosen for distinguishing between normal and abnormal variables that could be considered as anomalous according to (*Saunders and Potts 1976*). The result of applying this method is illustrated in the uranium point anomaly map (Fig. 21) which indicates the locations of areas exceeding ($X + 2S$) and ($X + 3S$) for eU, eU/eTh and eU/K variables. Careful examination of this map could lead to assignment that the uranium province zones are related to the three types of granite (G1, G2 and G3), the second type of Hammamat sediments (H2) and more or less to the acidic metavolcanics since they correspond to values of eU, eU/eTh and eU/K that exceeds ($X + 2S$) and ($X + 3S$).
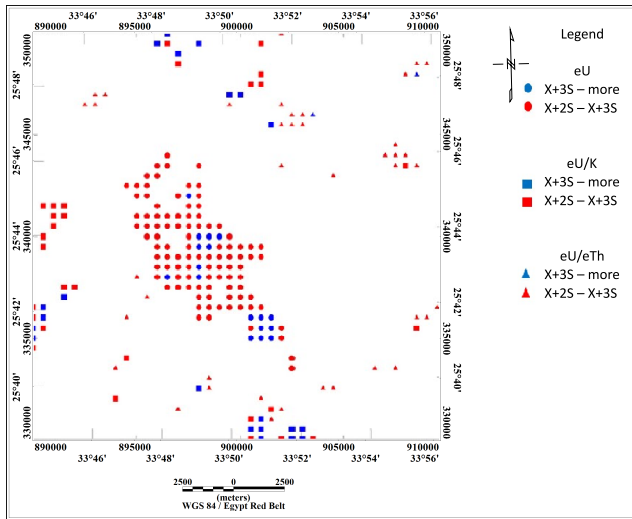

Fig. 21. The uranium point anomaly map of the study area.

3.2.4. Uranium migration

As a fact uranium and thorium are often associated in magma due to their similar ionic radius. However, uranium is active and easily to mobilize and

migrated under the action of oxygen from underground water and atmosphere during its evolution. Whereas thorium is relatively stable in oxidation zone, and stay in place as the result of breaking the original U-Th state. This means that the present Th-high area could be considered as the original U-high. Oxygen bearing ground water is effective uranium mobilizing agents. It can leach uranium dispersed in the rocks and uranium can later concentrate within sediments (*Benzing Uranium Institute, 1977*). The eU/eTh ratio is an important geochemical index for uranium migration; it is approximately constant in some types of rocks or geologic units in a relatively closed environment. On the other hand, the variations of uranium and thorium ratios reflect the extent of U migration in or out of this environment. The migration rate of uranium could be calculated according to the following equations (*Benzing Uranium Institute, 1977*):

$$\mathrm{Uo} = \mathrm{eTh} * \mathrm{eU/eTh}\,, \tag{1}$$

where, Uo: the original uranium content or paleo-uranium background, eTh: average of the eTh content in a certain geological unit in ppm, eU/eTh: average of regional eU/eTh ratio in different geological units.

$$\mathrm{Um} = \mathrm{Up} - \mathrm{Uo}\,, \tag{2}$$

where, Um: the amount of uranium migration or mobilized uranium, Up: the present average uranium content in a certain geologic unit.

$$\mathrm{P} = \mathrm{Um/Up} * 100\%\,, \tag{3}$$

where, P: the uranium migration rate.

As a fact there are two states of Um value: the first is, if the Um > 0, it reflects that uranium is migrated into the geologic body, the second is, if the Um < 0, it reflects that uranium is migrated out of the geologic body.

Accordingly, examination of the statistical results of uranium migration (Table 4), refers that uranium is migrated out from the majority of the nine rock units in the area of study. The amount of migrated uranium or mobilized uranium (Um) recorded negative values (Um < 0) in eight rock units out of nine units. The low negative values of Um values in the area may refer to the weak mobilization rate that is essentially due to the action of surface water. There is no clear high differentiation between the rates of migration from the exposed nine rock units in the study area. On the other

Table 4. Statistical results of uranium migration technique of the interpreted litho-radiometric units.

I.L.R.U.	Present uranium content (Up) * 0.1	Original uranium content (Uo) * 0.1	Migrated uranium (Um)	Uranium migration rate (P)
G1	28.23	28.852	−0.62	−2.19
G2	35.64	35.85	−0.209	−0.587
G3	21.60	22.26	−0.659	−3.055
H1	19.16	19.37	−0.204	−1.066
H2	13.50	13.43	0.072	0.538
A.M.V.	10.030	10.05	−0.0212	−0.212
I.M.V.	14.30	14.45	−0.145	−1.020
M.S.	8.34	8.37902	−0.03902	−0.46786
At. Fm.	17.45	17.57	−0.112	−0.644

Explanation: I.L.R.U. = interpreted litho-radiometric units, A.M.V. = acidic metavolcanics, At. Fm. = Attala Formation, G1 = Granite 1, G2 = Granite 2, G3 = Granite 3, H1 = Hammamat Formation-1, H2 = Hammamat Formation-2, I.M.V. = intermediate metavolcanics, M.S. = metasediments.

hand, the second type of the Hammamat sediments (H2) shows positive value of uranium migration (Um > 0.072) which means that uranium is migrated into this type with migration rate P = 0.538.

4. Conclusions

Airborne gamma-ray spectrometric surveys could be used for mapping the radioelements uranium, potassium and thorium in rocks because it is able to measure the chemical variation of radioactive elements (eU, K and eTh). So, like these surveys can contribute significantly to analysis and individualization of granitic intrusions. For these reasons, the aerial gamma-ray spectrometric data of Gabal El-Hassnawia granitic pluton have been analysed and processed with several techniques for interpretation. These techniques involved the surface lineaments analysis, qualitative description of radiometric maps, composite imaging, factor analysis, statistical treatment, mapping the interpreted litho-radiometric units and the uranium migration. The area of study enclosed between latitudes $25° 39' 00''$ & $25° 49' 20''$ N, and longitudes $33° 44' 30''$ & $33° 56' 15''$ E and comprises variety of sedimentary,

metamorphic and igneous rock types including metasediments, basic to intermediate and acidic metavolcanics, Hammamat sediments, Post Hammamat Felsites, younger granites and Quaternary sediments.

The well-developed structural elements of the area are oriented to NW, NNW, N–S and ENE trends and the main pluton has an oval shape and oriented mainly to NW direction. The qualitative description of the radiometric maps indicates that the younger granites possess the highest radiometric levels whereas the Hammamat sediments and the acidic metavolcanics have intermediate levels and the lowest levels of radioactivity are related to the metasediments, ultramafites and basic to intermediate metavolcanics.

The composite imaging proved that there is a good correlation between the concentration of radioelements and the mapped rock units. The bright higher concentration zones of the radioelement are clearly correlated with El-Hassnawia younger granite, two small poses to the east, Hammamat sediments and acidic metavolcanics. The black areas of low concentrations of eU, K and eTh indicate scattered small spots correlated with the metasediments, ultramafites and basic to intermediate metavolcanics.

The factor analysis proved that the three radioelements eU, K and eTh in addition to TC are highly correlated positively with each other recording scores of more than 95%. Three principal factors F1, F2 and F3 are extracted from the data and their scores were used in the radiometric differentiation between rock units. This technique assisted in recognizing nine interpreted litho-radiometric units. Three types of younger granites and two types of Hammamat sediments could be recognized among the nine units. These units are subjected to statistical treatment in order to identify the radiometric provinces of uranium occurrences that exceeds $X + 2S$ and $X + 3S$ as targets of exploration. Consequently, a point anomaly map was constructed and proved that the uranium province zones are related to the three types of granite (G1, G2 and G3), the second type of Hammamat sediments (H2) and more or less to the acidic metavolcanics.

Application of the uranium migration technique indicated that the second type of Hammamt sediments (H-2) is the only unit out of the nine units that characterize by uranium migration in, whereas, the uranium is migrated out acidic metavolcanics, Attala felsite, Granite-1, Granite-2, Granite-3, Hammamat sediments-1, basic to intermediate metavolcanics, and metasediments.

References

Abdel Gawad A. E., Ali K., Eliwa H., Sayyed M. I., Khandaker M. U., Bradley D. A., Osman H., Elesawy B. H., Hanfi M. Y., 2021: Radiological Investigation on Sediments: A Case Study of Wadi Rod Elsayalla the Southeastern Desert of Egypt. Appl. Sci., **11**, 24, 11884. 1–19, `doi: 10.3390/app112411884`.

Abu El Leil I., Waris M. A., Abdalla A. H., Attala A. F., Farage O., Said M., Ahmed A. M., El Ghazaly N. M., Ramadan A. M., Dyrenko V., Polyntsev Y., Ponomarje V. P., Nabrovenkov O., Belov Y., 1977: Results of prospecting for rare, nonferrous metals and gold in the area of wadis El Qash, Kareim and Zeidun in 1974-1975. (Report of Sebai Party 6/74). Unpublished report, Egyptian Geological Survey and Mining Authority, Cairo, Egypt, 151 p.

Aero-Service, 1984: Final operational report of airborne magnetic/radiation survey in the Eastern Desert, Egypt for the Egyptian General Petroleum Corporation. Aero-Service, Houston, Texas, April, 1984, Six Volumes.

Ahmed G. A. A., 2017: Tectonic evolution of the Precambrian rocks in the southern part of Wadi Attala, Central Eastern Desert, Egypt. MSc thesis, South Valley University, 179 p.

Ali M. A., Abdel Gawad A. E., Ghoneim M. M., 2021: Geology and mineral chemistry of uranium and thorium bearing minerals in rare-metal (NYF) pegmatites of Um Solimate, South Eastern Desert of Egypt. Acta Geol. Sin. (English edition), **95**, 5, 1568–1582, `doi: 10.1111/1755-6724.14708`.

Benzing Uranium Institute, 1977: Field Gamma- Ray spectrometric Survey No. 3, 1:292, China.

Broome H. J., 1990: Generation and interpretation of geophysical images with examples from the Rae Province, Northwestern Canada shield. Geophysics, **55**, 8, 977–997, `doi: 10.1190/1.1442927`.

Comery A. L., 1973: A first course in Factor Analysis. Academic Press, New York, 316 p.

Cordell L., Knepper D. H., 1987: Aeromagnetic images, fresh insight to the buried basement, Rolla Quadrangle, Southeast Missouri. Geophysics, **52**, 2, 218–231, `doi: 10.1190/1.1442297`.

Darnley A. G., 1973: Airborne gamma-ray survey techniques, present and future, in uranium exploration methods. Proceeding of panel; International Atomic Energy Agency, Venna, 67–108.

Darnley A. G., Ford K. L., 1989: Regional airborne gamma-ray surveys. A review. In: Garland G. D. (Ed.): Proceedingss of exploration '87, Third Decennial International Conference on Geophysical and Geochemical Exploration for Minerals and Groundwater, Ontario, Geological Survey of Canada, special 3, 960 p., 229–240.

Dessouky O. K., Dardier A. M., Abdel Ghani I. M., 2019: Egyptian Hammamat molasse basins and their relations to arc collision stages: Implications for radioactive elements mineralization potential. Geol. J., **54**, 3, 1205–1222, `doi: 10.1002/gj.3220`.

Duval J. S., 1976: Statistical interpretation of airborne gamma-ray spectrometric data using factor analysis. Proceeding of a symposium on exploration of uranium ore deposits. Vienna, IAEA. SM. 208/12.

Fowler A., Osman A. F., 2013: Sedimentation and inversion history of three molasse basins of the western central Eastern Desert of Egypt: Implications for the tectonic significance of Hammamat basins. Gondwana Res., **23**, 4, 1511–1534, `doi: 10.1016/j.gr.2012.08.022`.

Greiling R. O., De Wall H., Sadek M. F., Dietl C., 2014: Late Pan-African granite emplacement during regional deformation, evidence from magnetic fabric and structural studies in the Hammamat-Attala area, Central Eastern Desert of Egypt. J. Afr. Earth Sci., **99**, Part 1, 109–121, `doi: 10.1016/j.jafrearsci.2014.02.015`.

International Atomic Energy Agency (IAEA), 1976: Radiometric reporting methods and calibration in uranium exploration. Technical report series No. 174, Vienna.

International Atomic Energy Agency (IAEA), 1988: Geochemical exploration for uranium. Technical Reports Series, No. 284, IAEA, Vienna, Austria, 96 p.

Klovan J. E., 1968: Selection of target areas. A paper presented at the symposium on Decision-making in Exploration, Vancouver. January 26, 1968.

Mostafa M. E., 1988: Analysis of integrated geologic data for uranium exploration in Egypt. Case study, Tectonics of the structures bearing U-mineralization in the younger granitoids, Central Eastern Desert, Egypt. International Atomic Energy Agency (IAEA), Vienna, 172–184.

Mostafa M. E., Rabie S. I., El-Rakaiby M. L., 1990: Rock unit mapping using Factorial analysis applied to airborne gamma-ray spectrometric data, west Gabal Qattar Area, Egypt. Ann. Geol. Surv. Egypt, **XVI** (1986–1989), 295–300.

Mostafa M. E., Zakir F. A., 1996: New enhancement techniques for azimuthal analysis of lineaments for detecting tectonic trends in and around the Afro-Arabian Shield. Int. J. Remote Sens., **17**, 15, 2923–2943, `doi: 10.1080/01431169608949119`.

Osman A. F., 1996: Structural, geological and geochemical studies on the Pan-African basement rocks, wadi Zeidun, Central Eastern Desert, Egypt. Forschungszentrum Julich, Scientific Series of the International Bureau, **39**, 271 p.

Rabie S. I., Hussein A. H., Abdelnabi S. H., 1996: Distribution and interpretation of radioelements, Wadi Dib area, North Eastern Desert, Egypt. Proc. Egypt. Acad. Sci,. **46**, 469–502.

Sabet A. H., Polyntsev Y. M., Dyrenko V. A., 1976: Geological Map of Gebel El Sebai Sheet, Eastern Desert. Geol. Surv. Egypt.

Sarma D. D., Kock G. S., 1980: A statistical analysis of exploration geochemical data for uranium. Math. Geol., **12**, 2, 99–114, `doi: 10.1007/BF01035242`.

Saunders D. F., Potts M. J., 1976: Interpretation and application of high sensitivity airborne gamma ray spectrometric data. In: IAEA Symp. Exploration for Uranium Ore Deposits, Vienna, 107–124.

Wecksung G. W., 1982: A factor analysis approach for comparing aerial radiometrics with other related data sets. Geophysics, special research workshops, **47**, 4, 408–409.

Zoheir B., Feigenson M., Zi J.-W., Turrin B., Deshesh F., El-Metwally A., 2019: Ediacaran ($\sim$ 600 Ma) orogenic gold in Egypt: age of the Attala gold mineralization and its geological significance. Int. Geol. Rev., **61**, 7, 779–794, `doi: 10.1080/00206814.2018.1463180`.